BIOCHEMISTRY
including biophysical chemistry & molecular biology

Article

pubs.acs.org/biochemistry

Looking over Toxin−K^+ Channel Interactions. Clues from the Structural and Functional Characterization of α-KTx Toxin Tc32, a Kv1.3 Channel Blocker

Eliana G. Stehling,[†] Mauricio L. Sforça,[‡] Nilson I. T. Zanchin,[‡] Sérgio Oyama, Jr.,[‡] Angela Pignatelli,[§] Ottorino Belluzzi,[§] Eugenia Polverini,[∥] Romina Corsini,[⊥] Alberto Spisni,*[,⊥] and Thelma A. Pertinhez[⊥]

[†]Department of Toxicological and Bromatologic Clinical Analyses, Faculty of Pharmaceutical Sciences of Ribeirão Preto, USP, Ribeirão Preto, Brazil

[‡]National Laboratory of Biosciences, Campinas, Brazil

[§]Physiology and Biophysics Unit, Department of Biology and Evolution, University of Ferrara, Ferrara, Italy

[∥]Department of Physics, University of Parma, Parma, Italy

[⊥]Chemistry and Structural Biochemistry Unit, Department of Experimental Medicine, University of Parma, Parma, Italy

Supporting Information

ABSTRACT: α-KTx toxin Tc32, from the Amazonian scorpion *Tityus cambridgei*, lacks the dyad motif, including Lys27, characteristic of the family and generally associated with channel blockage. The toxin has been cloned and expressed for the first time. Electrophysiological experiments, by showing that the recombinant form blocks Kv1.3 channels of olfactory bulb periglomerular cells like the natural Tc32 toxin, when tested on the Kv1.3 channel of human T lymphocytes, confirmed it is in an active fold. The nuclear magnetic resonance-derived structure revealed it exhibits an α/β scaffold typical of the members of the α-KTx family. TdK2 and TdK3, all belonging to the same α-KTx 18 subfamily, share significant sequence identity with Tc32 but diverse selectivity and affinity for Kv1.3 and Kv1.1 channels. To gain insight into the structural features that may justify those differences, we used the recombinant Tc32 nuclear magnetic resonance-derived structure to model the other two toxins, for which no experimental structure is available. Their interaction with Kv1.3 and Kv1.1 has been investigated by means of docking simulations. The results suggest that differences in the electrostatic features of the toxins and channels, in their contact surfaces, and in their total dipole moment orientations govern the affinity and selectivity of toxins. In addition, we found that, regardless of whether the dyad motif is present, it is always a Lys side chain that physically blocks the channels, irrespective of its position in the toxin sequence.

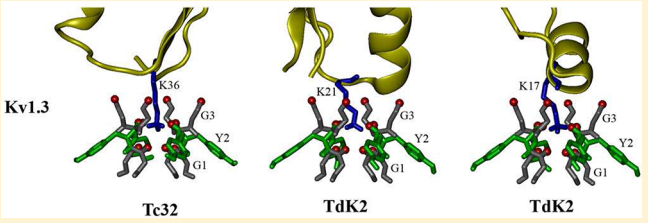

An increasing number of human autoimmune pathologies, such as type 1 diabetes mellitus, multiple sclerosis, rheumatoid arthritis, and allergic disorders, are associated with the activity of K^+ channels that control a wide range of T cell functions, including their activation. Thus, the pharmaceutical potential of molecules able to control K^+ channels is unmistakable.

More than 120 toxins isolated from scorpion venom selectively block K^+ channels.[1] Some of them exhibit nanomolar or picomolar affinity. Because of the impressive biodiversity of toxins and channels, to take maximal advantage of the pharmacological properties of the toxins, it is necessary to unravel the molecular determinants that control the selectivity and affinity of their channels. In this respect, the importance of the structural flexibility of both toxins and the channels in favoring a selective and high-affinity fit upon interaction is well-known.[2] Overall, it is accepted that the design of drugs aimed to control K^+ flux relies upon a detailed understanding of both the toxin fold and the contact surface between toxins and channels.

The main mechanism of action of toxins is physical pore blocking. The high-affinity binding for Kv channels was first associated with the presence, in the toxins, of a dyad motif formed by a hydrophobic residue (aromatic or aliphatic) flanking a lysine residue[3,4] and by specific amino acid side chains located in the outer vestibule of the channel.[1]

Some years ago, the functional dyad model was demonstrated not to be a prerequisite for toxin binding,[5] that indication being sustained by the discovery of toxin Tc32 isolated from the Amazonian scorpion *Tityus cambridgei*.[6] Tc32 belongs to the α-KTx group,[7] and it is the first member of the α-KTx 18 subfamily. Two others members of the α-KTx 18 subfamily, TdK2 and TdK3, were found in the venom of the scorpion *Tityus discrepans*.[8]

Received: November 15, 2011
Revised: February 14, 2012
Published: February 14, 2012

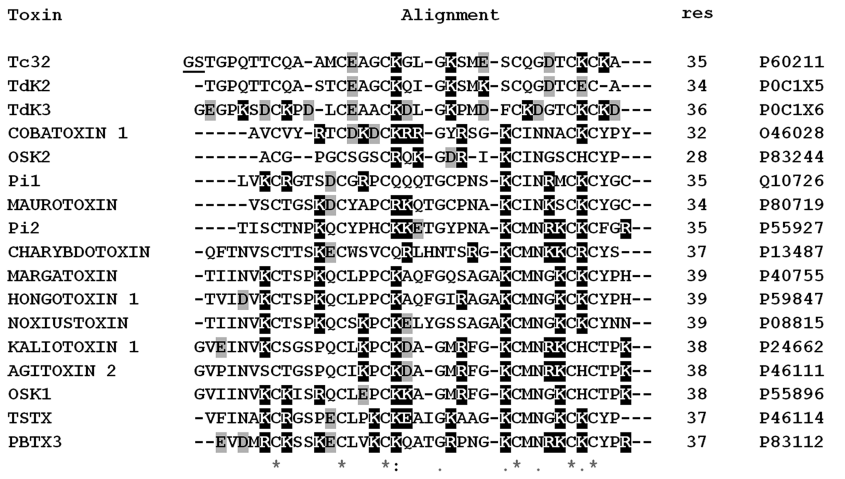

Figure 1. Amino acid sequence alignments of scorpion toxins using the ClustalW algorithm. The residue number and the Uniprot database code (http://www.uniprot.org) are indicated. The first three sequences represent the α-Ktx 18 subfamily. The positively charged residues are highlighted in black and the negatively charged residues in gray. Asterisks denote fully conserved residues (identity). Colons denote highly conserved residues. Periods denote weakly conserved residues. The sequence of recombinant Tc32 shows two additional residues, GS, in the N-terminus that are underlined (see Experimental Procedures).

Tc32 is a 35-residue peptide, containing three disulfide bonds, with a serine in place of K27 when compared to charybdotoxin (Figure 1), and it does not contain any aromatic residue. Although it lacks the dyad motif, Tc32 shows a clear inhibitory effect on Kv1.3 channels of human T lymphocytes: its affinity is in the nanomolar range, more than 2 orders of magnitude higher than its affinity for *Shaker* K^+ channels.[6]

Kv1.3 channels are involved in immune-mediated events that make them a key target in the design of immunosuppressive drugs for the treatment of allograft rejection and autoimmune diseases.[9] In addition, they carry a large proportion of the outward current in leucocytes[10,11] and in a variety of neuronal cells, including the interneurons (granule and non-dopaminergic periglomerular cells) of the olfactory bulb.[12]

In this work, Tc32 has been cloned and expressed in its active form for the first time, employing a protocol we devised.[13] Tc32 activity has been tested by electrophysiological assays on a distinct subpopulation of periglomerular cells of the olfactory bulb and its three-dimensional (3D) solution structure determined by ^{1}H NMR spectroscopy. On the basis of a structural and functional comparison with the other members of the α-KTx 18 subfamily, conducted following molecular modeling calculations and docking simulations for Kv1.1 and Kv1.3 channels, we suggest a novel general mechanism for toxin−channel interaction that we feel offers a new vision in the field.

EXPERIMENTAL PROCEDURES

Synthesis and Cloning of Oligonucleotide Probes of Toxin Tc32. The recombinant Tc32 toxin contains 37 amino acids (*GS*TGPQTTCQAAMCEAGCKGLGKS-MESCQGDTCKCKA), having two extra residues with respect to natural Tc32. In fact, the first two residues at the N-terminus, GS, originate from the *Bam*HI site used in the cloning protocol. Six oligonucleotide probes, whose sequences were 5′ gatccaccggcccgcagaccacctgccaggcggcgatgt 3′-3′ gtggccgggcgtctggtggacggtccgccgctacacgcttcgc 5′, 5′ gcgaagcgggctgcaaaggcctgggcaaaagcatgg 3′-3′ ccgacgtttccg-gacccgttttcgtacctttcgacg 5′, and 5′ aaagctgccagggcgatacctgcaaatg-caaagcgtaaa 3′-3′ gtcccgctatggacgtttacgtttcgcattttcga 5′, were used to clone the 105 bp of Tc32. Terminal fragments were flanked by *Bam*HI and *Hin*dIII sites at the 5′ and 3′ ends, respectively, to facilitate cloning into vector pTEV3,[13] a pET21-d-modified plasmid (gift from F. Bernard, University of Frankfurt, Frankfurt, Germany). A stop codon was also included at the 3′ end. DNA sequence analysis was conducted using a PE Biosystem model 377 DNA sequence with universal T7 promoter primers. The vector was then transformed into *Escherichia coli* strain BL21(DE3).

Protein Induction, Purification, and Matrix-Assisted Desorption Ionization Time-of-Flight (MALDI-TOF) Mass Spectrometry. The procedures for protein induction, purification, and MALDI-TOF mass spectrometry characterization followed a protocol previously described.[13] Briefly, protein expression was induced by the addition of 1 mM isopropyl β-D-thiogalactopyranoside (IPTG) to the culture broth; then the cells were harvested, disrupted by sonication, and centrifuged. The expressed protein was purified by affinity chromatography using a Ni-NTA superflow column and subsequently by ion exchange chromatography utilizing the HiTrap-Q column. The fractions containing the purified fusion proteins were treated with TEV protease to remove the D protein. Subsequently, the toxin was purified by reverse phase high-performance liquid chromatography (Shimadzu Co.) using a Vydac 218TP510 column. Elution was performed by applying a linear 0 to 100% acetonitrile gradient and 0.05% TFA over 100 min with an applied flow of 1 mL/min.

In agreement with the value expected for the presence of three disulfide bonds, the experimental Tc32 mass was 3666.4 Da.

Electrophysiological Measurements. *Animals, Surgical Procedures, and Cell Handling.* Experimental procedures were conducted to minimize animal suffering and the number of mice used. The procedures employed were in accordance with Directive 86/609/EEC on the protection of animals used for experimental and other scientific purposes and were approved by the Campus Veterinarian of the Ferrara University. A total of three mice were used.

Cell dissociation followed the procedure described in detail elsewhere[14] based on the protocol described by Gustincich and

co-workers.[15] Shortly after the bulbs had been dissected and sliced, small pieces of the preparation were transferred to a solution containing 0.3% protease type XXIII (Sigma) for 30−45 min at 37 °C. The protease activity was then arrested with 0.1% trypsin inhibitor (Sigma) (10 min, 37 °C), and the bulb chunks were triturated using fire-polished Pasteur pipettes of varying gauges. Finally, the dissociated cells were plated on glass coverslips coated with concanavalin A (1 mg/mL). More than 95% of the resulting cells were interneurons (granule and periglomerular cells), visually identified using differential interference contrast (DIC) microscopy. The projection neurons (mitral and tufted cells) usually did not survive the dissociation protocol and in any case could be easily identified for their dimensions and electrophysiological properties.

The cells were constantly perfused with physiological saline using a gravity flow system (2 mL/min) with a standard ACSF having the following composition: 125 mM NaCl, 2.5 mM KCl, 26 mM $NaHCO_3$, 1.25 mM NaH_2PO_4, 2 mM $CaCl_2$, 1 mM $MgCl_2$, and 15 mM glucose. Saline was continuously bubbled with a 95% O_2/5% CO_2 mixture; the osmolarity was adjusted at 305 mOsm with glucose. Cells were maintained for ∼15−20 min on average. All drugs and neuroactive compounds were purchased from Tocris (Bristol, U.K.), except tetrodotoxin (Alomone, Jerusalem, Israel). Drugs were bath applied, with a delay between valve opening and the onset of drug action of approximately 20 s.

The pipet filling solution contained 120 mM KCl, 10 mM NaCl, 2 mM $MgCl_2$, 0.5 mM $CaCl_2$, 5 mM EGTA, 10 mM HEPES, 2 mM Na-ATP, and 10 mM glucose; the osmolarity was adjusted at 295 mOsm with glucose, and the pH was set to 7.2 with NaOH.

Electrophysiological Methods. Macroscopic currents were recorded under whole-cell patch clamp with an Axopatch-200B amplifier (Molecular Devices, Sunnyvale, CA). The currents were sampled at 100 μs per point using a Digidata 1440A data acquisition system (Molecular Devices), filtered in-line at 5 kHz, and analyzed off-line using pClamp (Molecular Devices) and Microcal Origin (Origin Lab Corp., Northampton, MA). Leak conductance was subtracted with a P4 protocol;[16] off-line analysis was performed using version 10.2 of pClamp (Axon Instruments). The electrodes were pulled from borosilicate glass with an internal filament (Hilgenberg, 1.5 mm outside diameter, 0.87 mm inside diameter) to 4−4.5 MΩ resistance; 80% of the series resistance was electronically compensated.

Statistics. Data expressed as means ± the standard error of the mean were statistically analyzed using Origin version 7.5 with a paired *t*-test.

Circular Dichroism (CD). CD experiments were conducted on a Jasco 810 spectropolarimeter (Jasco Inc.) coupled to a Peltier Jasco PFD-425S system for temperature control. Tc32 was dissolved in water (pH 4.0) at a concentration of 80 μM. Far-UV spectra were recorded from 190 to 260 nm and averaged over four scans, using a 1 mm path-length quartz cell, in the temperature range of 6−86 °C. Following baseline correction, the observed ellipticity, θ (mgdeg), was converted to the molar mean residue ellipticity $[\theta]$ (deg cm^2 dmol^{-1}).

NMR Spectroscopy. Tc32 was dissolved in 600 μL of a 10% D_2O/90% H_2O mixture to yield a final concentration of 0.6 mM at pH 4.0. The NMR spectra were recorded using a Varian INOVA 600AS spectrometer at 15 °C. The two-dimensional proton homonuclear experiments were performed using the standard pulse sequence (see ref 17). Data were processed using NMRPipe/NMRView algorithms.[18,19] The NOE values were classified as strong, medium, and weak, corresponding to upper bound distances of 2.8, 3.5, and 5.0 Å, respectively. The lower bound was taken to be the sum of the van der Waals radii (1.8 Å) for the interacting protons.

Structure Calculations. Toxin models have been calculated using DYANA.[20] The structures with a target function smaller than 0.22 ± 0.02 Å^2, with no distance violation larger than 0.2 Å and with no dihedral angle violation grater than 5°, were energy minimized with full consistent valence force field[21] (Morse and Lennard-Jones potentials, Coulombic term) by steepest descents and conjugated gradient methods using several thousand iterations until the maximal derivative was less than 0.001 kcal mol^{-1} Å^{-1}. All calculations were conducted using DISCOVER (Accelrys, Inc.), together with Insight II as a graphic interface. Of the 40 starting structures, 18 models with the lower energies were selected for structural analysis using PROCHECK-NMR.[22]

Molecular Modeling. *Toxins.* The models of TdK2 and TdK3 were built by means of the Swiss-Model server,[23,24] using the minimized NMR-derived structure of the recombinant Tc32 as a template. In spite of the high percentage of residue identity (76% for TdK2 and 49% for TdK3), we preferred the modeling procedure with the largest amount of user intervention; therefore, after a multisequence alignment of the three sequences with ClustalW[25] (Figure 1), each of the two toxins was roughly built on the Tc32 template and then a refined model was requested from the server. The models obtained were further minimized with the Gromos96 force field[26] until a gradient of 10 kJ mol^{-1} Å^{-1} was reached. The quality of the structures was verified by the Swiss-Model structure assessment tools (including PROCHECK[27]), and the residue energy analysis was checked using the Gromos96 force field[26] and WhatCheck[28]. The electrostatic potential surfaces were calculated by means of the tools available in version 4.0.1 of Swiss PdbViewer,[29] using the Poisson−Boltzmann method, with atomic partial charges assigned following the Gromos96 force field parameter set,[26] at pH 7. The dielectric constant of the solvent was set to 80, and that of the interior of the protein was set to 4. An ionic strength of 150 mM was assumed as reported by Doyle and co-workers.[30] The equipotential contours have cutoffs of −1.6 k_bT/e for the negative value and 1.6 k_bT/e for the positive one, represented by colors that vary from red, through white (corresponding to 0 k_bT/e), to blue, respectively. The potential was mapped with the same color scheme to the solvent accessible surface, calculated with a rolling probe of radius 1.4 Å. The molecular dipole moment was calculated both by the Protein Dipole Moment Server of the Weizmann Institute[31] and by VMD[32] after atomic charges had been assigned with the PDB2PQR server,[33] according to the CHARMM force field.[34]

Kv Channels. The model structure of the human potassium Kv1.1 channel was obtained from Protein Data Bank (PDB)[35] entry 2afl. The structure of the Kv1.3 channel was built using the experimentally determined structure of bacterial *KcsA* (PDB entry 1J95[36]) as a template. The S5−S6 segment of Kv1.3, encompassing two transmembrane helices linked by the pore region, was aligned with the corresponding sequence of *KcsA*. On the basis of this alignment, 20 homology models were generated using MODELLER.[37] The resulting structures were internally checked by the scoring function of MODELLER and externally verified with PROCHECK.[27] The results were used to improve the alignment, and the cycle was repeated until a good stereochemical quality was achieved for the final model.

Docking Simulations. Although for the two α-KTx toxins TdK2 and TdK3 and for the K^+ channels we had only modeled structures (for Tc32 we had the experimental NMR-derived 3D structure), protein−protein docking simulations between each toxin and both Kv1.1 and Kv1.3 channels were attempted using the ClusPro2 server.[38,39] The 1000 best scoring results were clustered by the software on the basis of the ligand position, with a 9 Å Cα root-mean-square deviation (rmsd) radius for the cluster, and for each cluster, the "center" of the complex was shown.[40] The results were filtered on the basis of electrostatic interactions, accepting the notion it is the driving force for formation of the Ktx−Kv channel complex,[41] and because the hydrophobic interactions were highly biased by the hydrophobic surface of the channel that, *in vivo*, is embedded in the membrane.

All figures were created with VMD.[32]

RESULTS

Recombinant Toxin Tc32 Is an Active Toxin. To verify if the recombinant toxin Tc32 we produced was in an active fold, we tested its K^+ current blocking activity using the transient K^+ current present in granule and non-dopaminergic periglomerular cells of the mouse olfactory bulb. These cells are known to express Kv1.3 channels[42] based on functional[43−45] and immunohistochemical studies.[46,47] In particular, Kv1.3 channels have been localized in periglomerular cells[47] and in granule cells[12,44] of the olfactory bulb. Recordings were made from visually identified, enzymatically dissociated interneurons.

Only cells displaying a prominent fast transient K^+ current[45] were accepted for this study. The bulbar interneurons were voltage clamped in the whole-cell configuration at −100 mV and depolarized from −50 to 50 mV in 10 mV increments (Figure 2A). The sodium current was blocked with 1 μM TTX

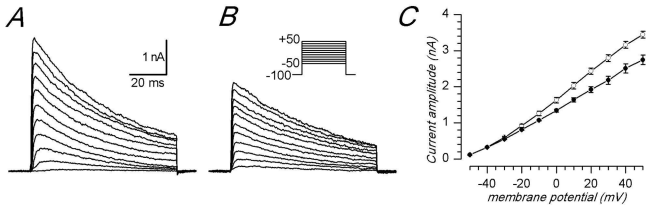

Figure 2. Effects of Tc32 on Kv1.3 K^+ channels in mouse interneurons (granule and periglomerular cells). (A) Macroscopic K^+ currents elicited by 80 ms pulses from a holding potential of −100 mV to test potentials ranging from −50 to 50 mV, in 10 mV increments, applied every 10 s. (B) Currents after the addition of 1 μM Tc32 to the external solution (pulse protocol as in panel A). (C) Peak current $I-V$ relationship of the complete set of traces: control (○) and toxin (●) at the test potentials (millivolts) (averaged data ± standard error); bars mark the variability that is significant at the 0.05% level (t-test).

to prevent any interference with the fast-developing K^+ current. The addition of 1.0 μM Tc32 to the extracellular solution blocked just ∼20% of the current carried by Kv1.3 channels (Figure 2B). The blockage could be reversed by perfusing the cell with the control ACSF solution (not shown). These effects are best seen in Figure 2C, which shows the complete $I-V$ relationships of the traces recorded of the average of four experiments described above: bars mark the variability that is significant at the 0.05% level (t-test). These results prove that the recombinant Tc32 inhibits Kv1.3 K^+ channels, thus indicating it exists in an active conformation.

CD Spectrum of Recombinant Tc32. The secondary structure of Tc32 was studied in the temperature range of 6−86 °C. The CD spectra exhibited a positive band at 190 nm and two negative bands at 205 and 222 nm, indicating the presence of helical structural elements (Figure 1S of the Supporting Information). The percentage of thermal unfolding, measured following the ellipticity at 205 and 222 nm, revealed that, at the maximal temperature reached, the toxin is not completely unfolded (Figure 1S of the Supporting Information and its inset), showing it possesses significant thermal stability.

NMR-Derived Structural Description. The spin systems were identified on the basis of both NOESY and TOCSY spectra, and the sequential assignment was obtained using the standard method.[48] Intraresidual HN−Hα cross-peaks were unambiguously assigned together with 98% of the other protons. The ^{1}H chemical shifts were deposited in the BioMagResBank as entry 15221.

The summary of the inter-residue NOEs for the toxin is reported in Figure 3. The presence of medium-range $d_{\alpha N}(i,i+3)$,

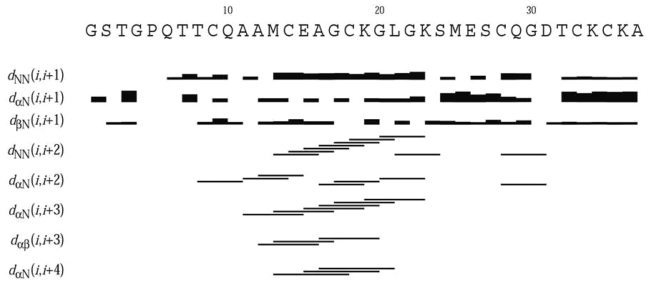

Figure 3. NOE pattern of the Tc32 toxin in a 90% H_2O/10% D_2O mixture at 15 °C and pH 4.0.

$d_{\alpha\beta}(i,i+3)$, and $d_{\alpha N}(i,i+4)$ NOEs, together with a strong $d_{NN}(i,i+1)$ NOE, indicates the existence of a helical element spanning residues A11−G20. The intense $d_{\alpha N}(i,i+1)$ NOEs between S24−C28 and T32−K36 and the low-intensity $d_{NN}(i,i+1)$ NOE indicate the presence of a two-strand β-sheet. It is worth noting that also in the N-terminal region we observe intense $d_{\alpha N}(i,i+1)$ NOEs (between the T3 and G4 pair and the T7 and T8 pair) and weak $d_{NN}(i,i+1)$ (between Q6 and T7) that could be indicative of a third β-strand. However, the presence of a proline at position 5 precludes a conclusive identification of a structural secondary element based only on the NOEs available. Nonetheless, the presence of the [...]C_1[...]C_2XXXC_3[...](G/A/S)XC_4[...]C_5XC_6 consensus sequence with the connection between pairs of half-cystines of the type C_1-C_4, C_2-C_5, and C_3-C_6 (C9−C28, C14−C33, and C18−C35, respectively), confirmed by NOEs, reminds of the scorpion charybdotoxin that has a $\beta\alpha\beta\beta$ type of fold and an α/β scaffold.[49,50] This structural identity supports the presence of the short N-terminal β-strand, thus conferring also to Tc32 a $\beta\alpha\beta\beta$ topology.

A total of 566 nonredundant distance restraints, of which 118 were medium- and long-range, were used for structure calculation using DYANA (Table 1). Of the 100 structures generated, 40 were selected on the basis of their minimal target function (<0.029 ± 0.008 Å^2) and energy-minimized using DISCOVER. After minimization, 18 structures were selected on the basis of the low residual distance violation of their backbone (0.24 ± 0.08 Å for T3−K36). The analysis of the Ramachandran plots for the ensemble of the calculated structures was conducted using PROCHECK-NMR[22] and

Table 1. Structural Statistics of the NMR-Derived Structures of Toxin Tc32

no. of structures	18
NOEs	
total no. of distance constraints	566
intraresidue	290
sequential	158
medium-range	74
long-range	44
Ramachandran plot analysis (%)	
most favored region	56.9
additionally allowed region	43.1
generously allowed region	0
disallowed region	0
rmsd	
backbone (residues)	global residues, 0.77 ± 0.21
	residues 3−36, 0.24 ± 0.08
heavy atoms (residues)	global residues, 0.99 ± 0.17
	residues 3−36, 0.73 ± 0.13

revealed 100% of the residues in favored regions. Overall, the statistics, the rmsd, and the Ramachandran plot, reported in Table 1, indicate the toxin has a well-defined structure.

The calculated structure of Tc32 shows the α/β-fold typical of members of the α-KTx family (Figure 4). It is characterized

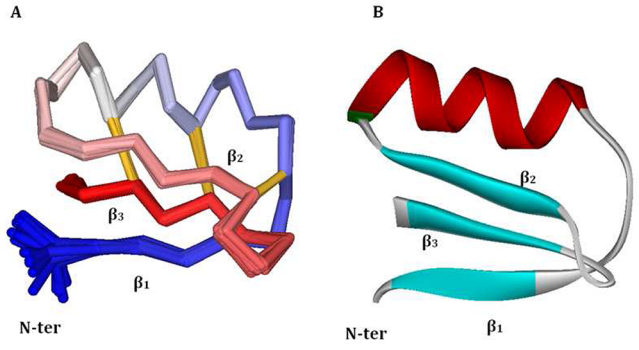

Figure 4. 3D structure of Tc32 toxin. (A) Superposition of the Cα backbone of the 18 selected models. Disulfide bonds are colored yellow. (B) Ribbon representation of the best conformer showing the α-helix in red (residues A11−G20) and the three-strand β-sheet in cyan (residues T3−Q6, S24−C28, and T32−K36).

by an α-helix spanning residues A11−G20, connected by two disulfide bridges, C14−C33 and C18−C35, to a three-strand antiparallel β-sheet formed by strands T3−Q6, S24−C28, and T32−K36. The third disulfide bridge, C9−C28, connects the β-sheet to a loop, residues T7−A10. The structure coordinates of Tc32 have been deposited as PDB entry 2JP6.

DISCUSSION

A multiple-sequence alignment of the three members of the α-KTx18 subfamily, performed with ClustalW,[25] shows 76% identity between recombinant Tc32 and TdK2 and 49% identity between recombinant Tc32 and TdK3 (Figure 1).

In spite of the similarity of their sequences, the toxins exhibit different selectivities for K^+ channels: Tc32 has a higher affinity for Kv1.3 than for Kv1.1, TdK2 acts on *Shaker* B (Kv1.1), and TdK3 is a poor blocker of both Kv1.3 and *Shaker* B channels.[6,8]

To verify that the different behaviors could be related to structural features, because no experimental structures are available for TdK2 and TdK3, we built their three-dimensional homology models, by means of comparative modeling techniques, using the NMR-derived structure of recombinant Tc32 as a template.

Structural and Electrostatic Features as Probes for Different Affinities and Selectivities. The models for TdK2 and TdK3 are shown in panels B and C of Figure 5, respectively. A 100 ns molecular dynamics simulation, in H_2O, was performed on each structure (including the NMR-derived structure of Tc32) to check their stability, which was confirmed (data not shown).

Each of the three toxins possesses a number of basic residues (Figure 5A−C) forming a sort of ring that, as already pointed out,[5,51] is expected to play a pivotal role in defining the toxins selectivity and affinity for Kv channels. In fact, those basic residues are found to form saline bridges with specific acidic residues located both in the filter region and on the turrets of the four channel subunits.

The three α-KTx 18 subfamily toxins exhibit a reduced net electric charge with respect to the other scorpion toxins (Figure 1). Tc32, with four basic and three acidic residues, has a net charge of +1, and TdK2, with three basic and three acidic residues, has a net charge of 0. TdK3, in spite of the largest number of charged residues, seven basic (all lysines) and eight acidic, has a net charge of −1.

The electrostatic potential (EP) surfaces of the toxins, calculated assuming an ionic strength of 150 mM, following the method of Doyle and co-workers,[30] are significantly different (Figure 5A′−C′). In particular, Tc32 presents a large basic surface near the K36 region. In the case of TdK2, we find three distinct, though equal in size and intensity, basic regions around the three lysine residues. Both in Tc32 and in TdK2, the surfaces of negative and positive potential are roughly separated in two regions of the molecule. The EP surface of TdK3, instead, does not show any well-defined charge separation because of the presence of a considerable number of positively and negatively charged amino acids sparsely distributed in the structure.

Besides the net electric charge and the EP surface, we evaluated the total dipole moment of the toxins, following the work on the scorpion toxin maurotoxin.[52] The total dipole moments of Tc32 and TdK2 are of the approximately same magnitude, while that of TdK3 is 3 times smaller. Its orientation in Tc32 is almost parallel to the side chains of K23 and K36; in TdK2, it aligns with the side chains of both K17 and K21, and in TdK3, it lines up with only K33 (Figure 5A−C). All dipole moments point outside the toxin core. As for Kv1.1 and Kv1.3 channels, their dipole moment is ∼10 times more intense than that of Tc32 and TdK2, and in both cases, it is oriented along the symmetry axis of the homotetramer, pointing toward the inner side of the membrane.

This diversity among the three toxins prompted us to investigate if it may be responsible for their dissimilar affinities and selectivities by influencing the interaction with the entry surface of the channels.

Hypothesis of a Common Channel−Toxin Interaction Mechanism. Scorpion toxin activity is not predominantly linked to its 3D architecture. In fact, in a manner independent of the ion channel type they target, the great majority presents an α/β-scaffold with a helix connected to a double- or triple-stranded β-sheet by two or three highly conserved disulfide bonds. Interestingly, however, because 80−90% of the amino acid side chains are surface-exposed, it is plausible that the type

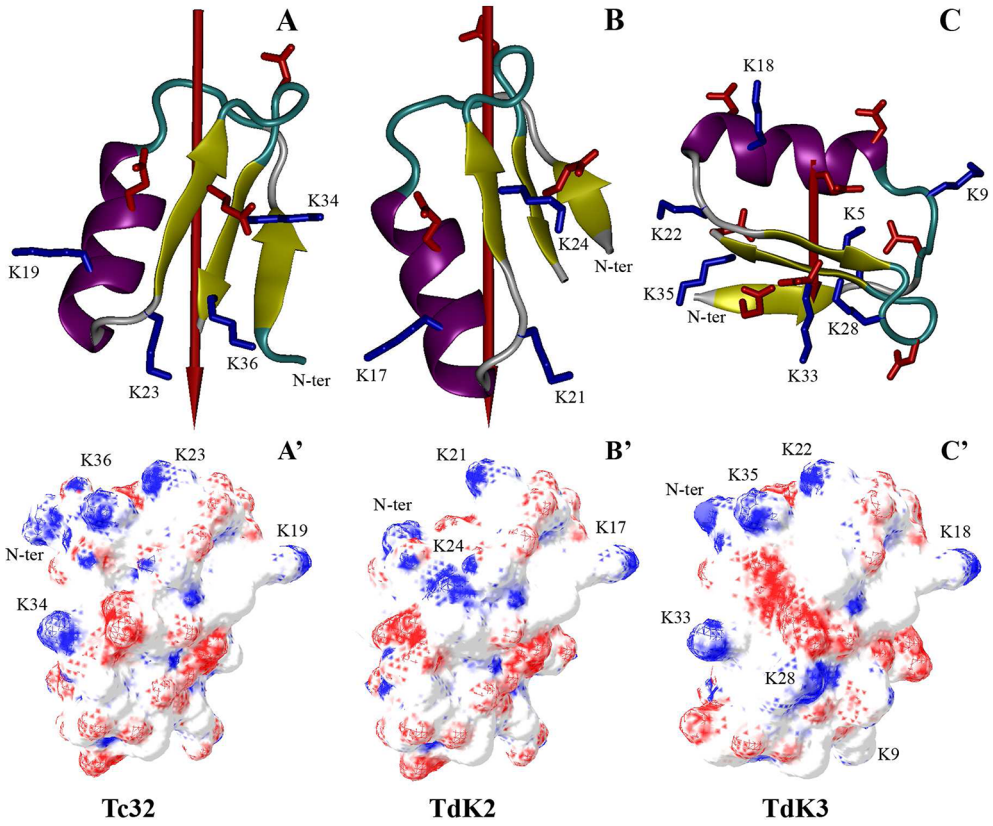

Figure 5. 3D structures of (A) Tc32, (B) TdK2, and (C) TdK3 toxins of the α-Ktx 18 subfamily (panels B and C are theoretical models). The models, in cartoon representations, are colored by secondary structure elements. Basic residues are shown as blue sticks and acidic residues as red ones. The dipole moment vector is drawn in red, pointing from negative to positive net charge. Its intensity is proportional to its length. The capital letters with primes represent the corresponding electrostatic potential surfaces of the molecules, calculated assuming an ionic strength of 150 mM.[30] The molecules are oriented differently with respect to the top panels, to better show the charge distributions and the protruding residues. The equipotential contours have cutoffs of -1.6 k_bT/e for the negative value and 1.6 k_bT/e for the positive one, represented by colors that go from red, through white (corresponding to 0 k_bT/e), to blue, respectively. The potential was mapped with the same color scheme to the solvent accessible surface, calculated with a rolling probe radius of 1.4 Å.

and position of the residues have to be critical. Indeed, it is widely accepted that subtle differences in the toxin−channel contact surface are responsible for their diverse selectivity and affinity.[53] Thus, point mutations and/or alteration of the spatial orientation of a side chain either in the K^+ channels or in the toxins may modify their reciprocal affinity.

Although we recognize that, in this study, the structures of the toxins (with the exception of Tc32) and the channels are theoretical models, in other words low-resolution structures, to dissect the structural features responsible for the interaction of the three selected toxins with Kv channels we conducted protein−protein docking simulations. Each of the three toxins was docked to the Kv1.1 and Kv1.3 K^+ channel by means of the ClusPro2 webserver.[38,39] The electrostatically driven interactions lead to energetically favorable complexes in which, despite the fact that the toxins do not present the classic dyad or the K27 conserved residue of charybdotoxin, a lysine residue inserts into the channel pore at the selectivity filter level (Figure 6 and Figure 2S of the Supporting Information) as in other toxins:[2,5,41,54,55] in other words, in the absence of the canonical dyad partner, a lysine residue, even when located in a position different from that of the significantly conserved K27,[2,5,41,54,55] can physically block the extracellular entryway of the channel.

In agreement with the current model of toxin−Kv interaction, in both Tc32− and TdK2−Kv complexes, the lysine side chain that inserts into the pore interacts closely with the main chain oxygen atoms of the conserved selectivity filter residues G-Y-G (the K^+ channel signature sequence), which line the pore surface and are involved in the conduction of K^+ ions[30] (Figure 6).

It is worth noting, however, that in all favorable complexes of Tc32 with both types of channels only K36 is involved (Figure 2S A,A′ of the Supporting Information), even if the four lysine residues have their side chains preferentially extended outward and potentially suited to insert into the pore. Noteworthy is the fact that the orientation of the Tc32 dipole moment turns out to be parallel to the K36 side chain (Figure 5A) and consequently to the channel dipole moment. As reported by Blanc and co-workers,[52] the alignment of the two dipoles is the favorable condition for interaction and, even better, the factor that guides and orients the toxin into the pore. Following this rationale, we can explain why, though the Tc32 dipole moment is also parallel to the K23 side chain (Figure 5A), no complex is found with that residue inserted into the channel pore. Inspection of the structural models available shows that K23 has a reduced protruding surface (Figure 5A′) that makes it less suited for insertion into the pore; in addition, the EP of its neighborhood is more negative than for K36 (Figure 5A′), and it hampers the contacts with the acidic channel mouth.

The TdK2 favorable complexes show that the side chains of two of three lysines, K17 and K21, alternatively insert into the pore (Figure 2S B,B′,C,C′ of the Supporting Information), in

dx.doi.org/10.1021/bi201713z | *Biochemistry* 2012, 51, 1885−1894

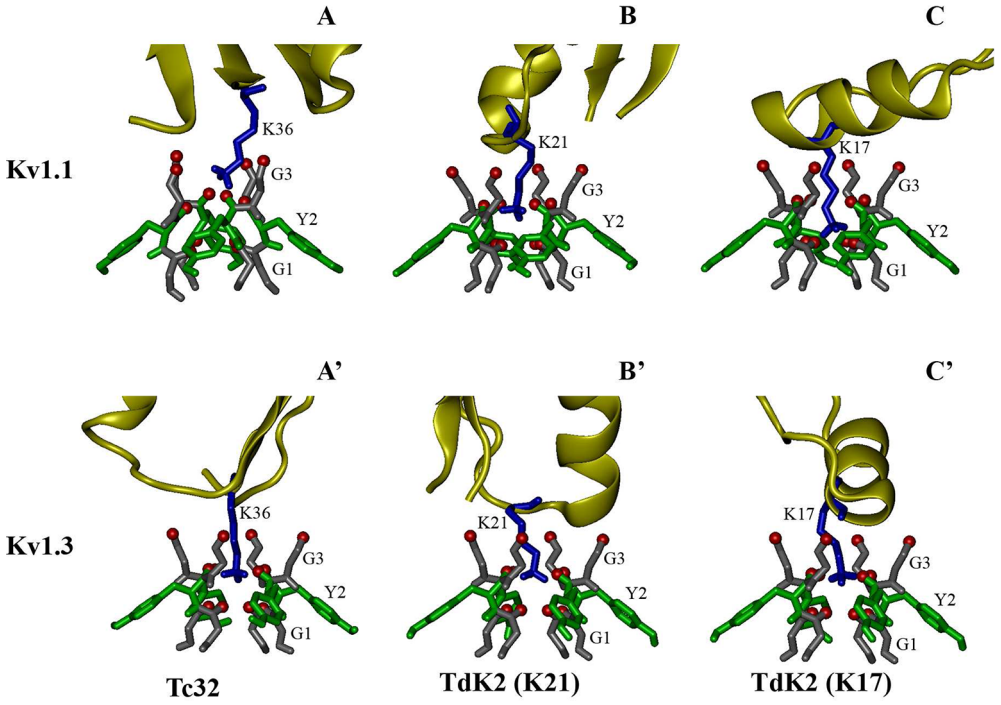

Figure 6. Close-up view of the interactions of the lysine residue (blue stick) in the pore and the channel G-Y-G residues (glycines colored silver, tyrosines colored green): (A and A′) Tc32, (B and B′) TdK2 with the K21 residue in the pore, and (C and C′) TdK2 with the K17 residue in the pore. The Kv1.1 channel complexes are shown in the top row, while the Kv1.3 channel complexes are shown in the bottom row. The oxygen atoms of these residues that line the pore surface and interact with the lysine side chain head are highlighted in red.

agreement with the observed orientation of the dipole moment of TdK2, almost parallel to the side chains of both lysines (Figure 5B) and therefore to the channel dipole. As for the side chain of the third lysine residue, K24, not only it is not aligned to the total dipole moment but, in addition, it establishes contacts with the negatively charged C-terminus and other acidic side chains of the toxin: these unfavorable structural features inhibit its insertion into the pore. Interestingly, the experimentally determined affinity data[6,8] that show for TdK2 a stronger capability to block the Kv1.1 channels than Tc32 can be justified by TdK2 having two equivalent lysines that can insert into the pore (K17 and K21).

Finally, though TdK3 has the side chains of all its lysines extended outward, it does not show any favorable complex with a lysine inside the entry pore of Kv1.1, and only one with Kv1.3. Certainly, we may expect that the significant number of negatively charged residues (Figure 5C′) hinders the interaction of the toxin with the negatively charged channel entryway surface. However, the analysis of the dipole moment provides additional clear hints that justify the computational results: it is 3 times smaller than those of the other two toxins, and it is properly aligned with respect to only one lysine, K33. In fact, the other lysines turn out to be either almost perpendicular (K9, K22, K28, and K35) or antiparallel (K5 and K18), implying that if they would enter the pore the toxin dipole would be misaligned with respect to the channel dipole. Overall, the ensemble of these considerations provides independent support for the docking results and justifies the very poor blocking ability of TdK3.

The mechanistic model we propose is supported by the observation that, in all complexes of Tc32 and TdK2 with both Kv1.1 and Kv1.3 channels, the positively charged region surrounding the pore-plugging lysine interacts with the negatively charged residues of the turrets (Figure 2S of the Supporting Information), securing the toxin in place and the lysine into the pore as postulated previously.[5,51]

Our docking results provide also the grounds for some speculation about the structural features that might help to explain the differences in the selectivity of the toxins toward Kv1.1 and Kv1.3 channels, in particular with respect to Tc32, for which a whole set of experimental data is available.[6] The conserved selectivity filter, G-Y-G, corresponds (from the inside to the outside of the pore) to G374, Y375, and G376 in Kv1.1 and to G446, Y447, and G448 in Kv1.3 [from UniProt entries Q09470 and P22001, respectively (http://www.uniprot.org)]. For the sake of clarity, we will denote them as G1, Y2, G3, respectively, where G1 is the inner glycine and G3 the outer one (Figure 6).

In all found complexes, K36 of Tc32 penetrates more deeply into the pore of Kv1.3 than of Kv1.1. That differential localization can be explained by a strong interaction with the main chain oxygen atoms of G1 and Y2 of the four subunits of Kv1.3 (Figure 6A). In the case of Kv1.1, the side chain of K36 interacts preferentially with the oxygen atoms of outer residues Y2 and G3 (Figure 6A′). Thus, the higher affinity for Kv1.3 is consistent with the model postulated by Lange and coworkers,[2] in which high-affinity binding is related to a deeper insertion of the lysine side chain into the selectivity filter. We hypothesize that the depth of penetration is controlled by conformational and chemical features of the turret side chains that are complementary to those of the residues surrounding the lysines of the toxin.

In the case of TdK2, the position inside the pore of K17 and K21 is the same in both channels: the side chains of the two lysines interact with the main chain oxygens of residues G1 and Y2 (Figure 6B,B′,C,C′). Interestingly, in Kv1.3, at least for K17, the side chain enters more deeply inside the selectivity filter than K36 of Tc32. These observations are consistent with the

dx.doi.org/10.1021/bi201713z | *Biochemistry* 2012, 51, 1885−1894

lower dissociation constant measured for TdK2 versus that of Tc32, when tested against the Kv1.1 channel.

Because of the lack of experimental affinity data for the interaction of TdK2 with Kv1.3 and the current extreme difficulty in obtaining natural scorpion toxins, we are now progressing in the production of recombinant TdK2 and Tc32 variants to validate our model.

CONCLUSIONS

Here we present a model in which the physical blockade of Kv1.*x* channels by means of a lysine side chain, because of its structural (long and thin) and electrostatic (positively charged) features that make it ideal for penetrating into the channel's pore, appears to be a common feature of α-KTx toxins also in the absence of the dyad motif.[5,6,52]

The usefulness of toxins in biomedical research, diagnosis, and therapy is widely recognized. Unfortunately, their use is limited by inadequate target discrimination. Thus, the search for target-specific toxins is of primary relevance. The fact that despite the incredible number of toxins present in the animal kingdom, only a very limited variety of molecular scaffolds has been selected,[56] is clear evidence of the importance of the nature and spatial orientation of the side chains. This consideration is strengthened by the observation that toxins are generally small polypeptides, 20−100 residues at most, a fact that allows most of the side chains to point outward. Following this rationale, the description and understanding of the contact surface between a toxin and the channel entrance appear to be the target for the rationale design of novel channel blockers that may turn into selective and high-affinity drugs. To support this goal, recognizing that a correlation exists between toxin affinity and specificity and the magnitude and orientation of its dipole moment,[52] we found this molecular feature turns out to be a very useful tool for predicting the residues interacting with the channel pore.

Overall, this work further supports the notion that a thorough analysis of the toxin−channel contact surface can provide a rationale for understanding their selectivity and affinity.

ASSOCIATED CONTENT

Supporting Information

Tc32 CD spectra and overall view of the complexes of Tc32 and TdK2 toxins with both Kv1.1 and Kv1.3 potassium channels. This material is available free of charge via the Internet at http://pubs.acs.org.

AUTHOR INFORMATION

Corresponding Author

*Department of Experimental Medicine, University of Parma, Via Volturno, 39, 43125 Parma, Italy. E-mail: alberto.spisni@unipr.it. Telephone: +39 0521 033807. Fax: +39 0521 033802.

Funding

Supported by grants from FAPESP, Brazil, to A.S. (99/11030-9, 99/07574-3, and 00/10266-8). E.G.S. (03/01921-0) and M.L.S. (01/08095-3) were recipients of postdoctoral fellowships. T.A.P. (00/02026-7) was a recipient of a Career Award Fellowship.

Notes

The authors declare no competing financial interest.

ACKNOWLEDGMENTS

We thank Prof. Dr. Frank Bernard (Johann Wolfgang Goethe Universität, Frankfurt, Germany) for providing us with plasmid pTEV3.

ABBREVIATIONS

ACSF, artificial cerebrospinal fluid; CD, circular dichroism; EP, electrostatic potential; NMR, nuclear magnetic resonance; OBPC, olfactory bulb periglomerular cells.

REFERENCES

(1) Rodriguez de la Vega, R. C., and Possani, L. D. (2004) Current views on scorpion toxins specific for K^+-channels. *Toxicon 43*, 865−875.

(2) Lange, A., Giller, K., Hornig, S., Martin-Eauclaire, M.-F., Pongs, O., Becker, S., and Baldus, M. (2006) Toxin-induced conformational changes in a potassium channel revealed by solid-state NMR. *Nature 440*, 959−962.

(3) Possani, L. D., Selisko, B., and Gurrola, G. B. (1999) Structure and function of scorpion toxins affecting K^+ channels. In *Perspectives in Drug Discovery and Design: Animal Toxins and Potassium Channels*, 15/16, pp 15−40, Kluwer/Escom, Dordrecht, The Netherlands.

(4) Mouhat, S. (2008) Animal toxins acting on voltage-gated potassium channels. *Curr. Pharm. Des. 14*, 2503−2518.

(5) Mouhat, S., Mosbah, A., Visan, V., Wulff, H., Delepierre, M., Darbon, H., Grissmer, S., De Waard, M., and Sabatier, J. M. (2004) The "functional" dyad of scorpion toxin P1 is not itself a prerequisite for toxin binding to the voltage-gated Kv1.2 potassium channels. *Biochem. J. 377*, 25−36.

(6) Batista, C. V. F., Gómez-Lagunas, F., de la Vega, R. C. R., Hajdu, P., Panyi, G., Gáspar, R., and Possani, L. D. (2002) Two novel toxins from the Amazonian scorpion *Tityus cambridgei* that block Kv1.3 and Shaker B K^+-channels with distinctly different affinities. *Biochim. Biophys. Acta 1601*, 123−131.

(7) Tytgat, J., Chandy, K. G., Garcia, M. L., Gutman, G. A., Martin-Eauclaire, M. F., Van der Walt, J. J., and Possani, L. D. (1999) A unified nomenclature for short-chain peptides isolated from scorpion venoms: α-KTx molecular subfamilies. *Trends Pharmacol. Sci. 11*, 444−447.

(8) Batista, C. V. F., D'Suze, G., Gómez-Lagunas, F., Zamudio, F. Z., Encarnacion, S., Sevcik, X., and Possani, L. D. (2006) Proteomic analysis of *Tityus discrepans* scorpion venom and amino acid sequence of novel toxins. *Proteomics 6*, 3718−3727.

(9) Beeton, C., Wulff, H., Standifer, N. E., Azam, P., Mullen, K. M., Pennington, M. W., Kolski-Andreaco, A., Wei, E., Grino, A., Counts, D. R., Wang, P. H., LeeHealey, C. J., Andrews, B. S., Sankaranarayanan, A., Homerick, D., Roeck, W. W., Tehranzadeh, J., Stanhope, K. L., Zimin, P., Havel, P. J., Griffey, S., Knaus, H. G., Nepom, G. T., Gutman, G. A., Calabresi, P. A., and Chandy, K. G. (2006) Kv1.3 channels are a therapeutic target for T cell-mediated autoimmune diseases. *Proc. Natl. Acad. Sci. U.S.A. 103*, 17414−17419.

(10) Yellen, G. (2002) The voltage-gated potassium channels and their relatives. *Nature 419*, 35−42.

(11) Beeton, C., and Chandy, K. G. (2005) Potassium channels, memory T cells, and multiple sclerosis. *Neuroscientist 11*, 550−562.

(12) Fadool, D. A., and Levitan, I. B. (1998) Modulation of olfactory bulb neuron potassium current by tyrosine phosphorylation. *J. Neurosci. 18*, 6126−6137.

(13) Stehling, E. G., da Silveira, W. D., Campos, T. A., Brocchi, M., Pertinhez, T. A., and Spisni, A. (2008) Development of a bacterial cloning vector for expression of scorpion toxins for biotechnological studies. *Protein Expression Purif. 57*, 88−94.

(14) Pignatelli, A., and Belluzzi, O. (2008) Cholinergic modulation of dopaminergic neurons in the mouse olfactory bulb. *Chem. Senses 33*, 331−338.

(15) Gustincich, S., Feigenspan, A., Wu, D. K., Koopman, L. J., and Raviola, E. (1997) Control of dopamine release in the retina: A transgenic approach to neural networks. *Neuron 18*, 723−736.
(16) Armstrong, C. M., and Bezanilla, F. (1974) Charge movement associated with the opening and closing of the activation gates of the Na channels. *J. Gen. Physiol. 63*, 533−552.
(17) Oyama, S. Jr., Pristovšek, P., Franzoni, L., Pertinhez, T. A., Schininá, E., Lücke, C., Rüterjans, H., Arantes, E. C., and Spisni, A. (2005) Probing the pH-dependent structural features of α-KTx12.1, a potassium channel blocker from the scorpion *Tityus serrulatus*. *Protein Sci. 14*, 1025−1038.
(18) Delaglio, F., Grzesiek, S., Vuister, G. W., Zhu, G., Pfeifer, J., and Bax, A. (1995) NMRPipe: A multidimensional spectral processing system based on UNIX pipes. *J. Biomol. NMR 6*, 277−293.
(19) Johnson, B., and Blevins, R. A. (1994) NMRView: A computer program for the visualization and analysis of NMR data. *J. Biomol. NMR 4*, 603−614.
(20) Güntert, P., Mumenthaler, C., and Wüthrich, K. (1997) Torsion angle dynamics for NMR structure calculation with the new program DYANA. *J. Mol. Biol. 273*, 283−298.
(21) Dauber-Osguthorpe, P., Roberts, V. A., Osguthorpe, D. J., Wolff, J., Genest, M., and Hagler, A. T. (1988) Structure and energetics of ligand binding to proteins: *Escherichia coli* dihydrofolate reductase-trimethoprim, a drug-receptor system. *Proteins 4*, 31−47.
(22) Laskowski, R. A., Rullmannn, J. A., MacArthur, M. W., Kaptein, R., and Thornton, J. M. (1996) AQUA and PROCHECK-NMR: Programs for checking the quality of protein structures solved by NMR. *J. Biomol. NMR 8*, 477−486.
(23) Schwede, T., Kopp, J., Guex, N., and Peitsch, M. C. (2003) SWISS-MODEL: An automated protein homology-modeling server. *Nucleic Acids Res. 31*, 3381−3385.
(24) Arnold, K., Bordoli, L., Kopp, J., and Schwede, T. (2006) The SWISS-MODEL workspace: A web-based environment for protein structure homology modelling. *Bioinformatics 22*, 195−201.
(25) Chenna, R., Sugawara, H., Koike, T., Lopez, R., Gibson, T. J., Higgins, D. G., and Thompson, J. D. (2003) Multiple sequence alignment with the Clustal series of programs. *Nucleic Acids Res. 31*, 3497−3500.
(26) Van Gunsteren, W., Billeter, S., Eising, A., Hunenberger, P., Kruger, P., Mark, A., Scott, W., and Tironi, I. (1996) *Biomolecular simulation: The GROMOS96 Manual and User Guide*, Vdf Hochschulverlag, Zurich.
(27) Laskowski, R. A., MacArthur, M. W., Moss, D. S., and Thornton, J. M. (1993) PROCHECK: A program to check the stereochemical quality of protein structures. *J. Appl. Crystallogr. 26*, 283−291.
(28) Hooft, R. W., Vriend, G., Sander, C., and Abola, E. E. (1996) Errors in protein structures. *Nature 381*, 272.
(29) Guex, N., and Peitsch, M. C. (1997) SWISS-MODEL and the Swiss-PdbViewer: An environment for comparative protein modeling. *Electrophoresis 18*, 2714−2723.
(30) Doyle, D. A., Cabral, J. M., Pfuetzner, R. A., Kuo, A., Gulbis, J. M., Cohen, S. L., Chait, B. T., and MacKinnon, R. (1998) The structure of the potassium channel: Molecular basis of K^+ conduction and selectivity. *Science 280*, 69−77.
(31) Felder, C. E., Prilusky, J., Silman, I., and Sussman, J. L. (2007) A server and database for dipole moments of proteins. *Nucleic Acids Research*, Vol. *35*, Oxford University Press, New York (http://bioinfo.weizmann.ac.il/dipol/).
(32) Humphrey, W., Dalke, A., and Schulten, K. (1996) VMD: Visual molecular dynamics. *J. Mol. Graphics 14*, 33−38.
(33) Dolinsky, T. J., Nielsen, J. E., McCammon, J. A., and Baker, N. A. (2004) PDB2PQR: An automated pipeline for the setup of Poisson-Boltzmann electrostatics calculations. *Nucleic Acids Res. 32*, W665−W667.
(34) MacKerell, A. D. Jr., Bashford, D., Bellott, M., Dunbrack, R. L. Jr., Evanseck, J. D., Field, M. J., Fischer, S., Gao, J., Guo, H., Ha, S., Joseph-McCarthy, D., Kuchnir, L., Kuczera, K., Lau, F. T. K., Mattos, C., Michnick, S., Ngo, T., Nguyen, D. T., Prodhom, B., Reiher, W. E. III, Roux, B., Schlenkrich, M., Smith, J. C., Stote, R., Straub, J., Watanabe, M., Wiórkiewicz-Kuczera, J., Yin, D., and Karplus, M. (1998) All-atom empirical potential for molecular modeling and dynamics studies of proteins. *J. Phys. Chem. B 102*, 3586−3616.
(35) Berman, H. M., Westbrook, J., Feng, Z., Gilliland, G., Bhat, T. N., Weissig, H., Shindyalov, I. N., and Bourne, P. E. (2000) The Protein Data Bank. *Nucleic Acids Res. 28*, 235−242.
(36) Zhou, M., Morais-Cabral, J. H., Mann, S., and MacKinnon, R. (2001) Potassium channel receptor site for the inactivation gate and quaternary amine inhibitors. *Nature 411*, 643−644.
(37) Šali, A., and Blundell, T. L. (1993) Comparative protein modelling by satisfaction of spatial restraints. *J. Mol. Biol. 234*, 779−815.
(38) Kozakov, D., Hall, D. R., Beglov, D., Brenke, R., Comeau, S. R., Shen, Y., Li, K., Zheng, J., Vakili, P., Paschalidis, I. C., and Vajda, S. (2010) Achieving reliability and high accuracy in automated protein docking: ClusPro, PIPER, SDU, and stability analysis in CAPRI rounds 13−19. *Proteins: Struct., Funct., Bioinf. 78*, 3124−3130.
(39) Comeau, S. R., Gatchell, D. W., Vajda, S., and Camacho, C. J. (2004) ClusPro: An automated docking and discrimination method for the prediction of protein complexes. *Bioinformatics 20*, 45−50.
(40) Kozakov, D., Clodfelter, K., Vajda, S., and Camacho, C. (2005) Optimal clustering for detecting near-native conformations in protein docking. *Biophys. J. 89*, 867−875.
(41) Chen, P., and Kuyucak, S. (2009) Mechanism and energetics of charybdotoxin unbinding from a potassium channel from molecular dynamics simulations. *Biophys. J. 96*, 2577−2588.
(42) Gutman, G. A., Chandy, K. G., Grissmer, S., Lazdunski, M., McKinnon, D., Pardo, L. A., Robertson, G. A., Rudy, B., Sanguinetti, M. C., Stuhmer, W., and Wang, X. (2005) International Union of Pharmacology. LIII. Nomenclature and molecular relationships of voltage-gated potassium channels. *Pharmacol. Rev. 57*, 473−508.
(43) Bardoni, R., Puopolo, M., Magherini, P. C., and Belluzzi, O. (1996) Potassium currents in periglomerular cells of frog olfactory bulb in vitro. *Neurosci. Lett. 210*, 95−98.
(44) Fadool, D. A., Tucker, K., Perkins, R., Fasciani, G., Thompson, R. N., Parsons, A. D., Overton, J. M., Koni, P. A., Flavell, R. A., and Kaczmarek., L. K. (2004) Kv1.3 channel gene-targeted deletion produces "Super-Smeller Mice" with altered glomeruli, interacting scaffolding proteins, and biophysics. *Neuron 41*, 389−404.
(45) Puopolo, M., and Belluzzi, O. (1998) Functional heterogeneity of periglomerular cells in the rat olfactory bulb. *Eur. J. Neurosci. 10*, 1073−1083.
(46) Serodio, P., and Rudy, B. (1998) Differential expression of Kv4 K^+ channel subunits mediating subthreshold transient K^+ (A-type) currents in rat brain. *J. Neurophysiol. 79*, 1081−1091.
(47) Veh, R. W., Lichtinghagen, R., Sewing, S., Wunder, F., Grumbach, I. M., and Pongs, O. (1995) Immunohistochemical localization of five members of the Kv1 channel subunits: Contrasting subcellular locations and neuron-specific co-localizations in rat brain. *Eur. J. Neurosci. 7*, 2189−2205.
(48) Wüthrich, K. (1986) *NMR of Proteins and Nucleic Acids*, John Wiley & Sons, Inc., Zurich.
(49) Bontems, F., Roumestand, C., Gilquin, B., Ménez, A., and Toma, F. (1991) Refined structure of charybdotoxin: Common motifs in scorpion toxins and insect defensins. *Science 254*, 1521−1523.
(50) Bontems, F., Gilquin, B., Roumestand, C., Ménez, A., and Toma, F. (1992) Analysis of side-chain organization on a refined model of charybdotoxin: Structural and functional implications. *Biochemistry 31*, 7756−7764.
(51) Jouirou, B., Mouhat, S., Andreotti, N., De Waard, M., and Sabatier, J. M. (2004) Toxin determinants required for interaction with voltage-gated K^+ channels. *Toxicon 43*, 909−914.
(52) Blanc, E., Sabatier, J. M., Kharrat, R., Meunier, S., el Ayeb, M., Van Rietschoten, J., and Darbon, H. (1997) Solution structure of maurotoxin, a scorpion toxin from *Scorpio maurus*, with high affinity for voltage-gated potassium channels. *Proteins 29*, 321−333.
(53) Rodríguez de la Vega, R. C., Merino, E., Becerril, B., and Possani, L. D. (2003) Novel interactions between K^+ channel and scorpion toxins. *Trends Pharmacol. Sci. 24*, 222−227.

(54) Miller, C. (1995) The charybdotoxin family of K^+ channel-blocking peptides. *Neuron 15*, 5−10.
(55) Jouirou, B., Mosbah, A., Visan, V., Grissmer, S., M'Barek, S., Fajloun, Z., Van Rietschoten, J., Devaux, C., Rochat, H., Lippens, G., El Ayeb, M., De Waard, M., Mabrouk, K., and Sabatier, J. M. (2004) Cobatoxin 1 from *Centruroides noxius* scorpion venom: Chemical synthesis, three-dimensional structure in solution, pharmacology and docking on K^+ channels. *Biochem. J. 377*, 37−49.
(56) Fry, B. G., Roelants, K., Champagne, D. E., Scheib, H., Tyndall, J. D. A., King, G. F., Nevalainen, T. J., Norman, J. A., Lewis, R. J., Norton, R. S., Renjifo, C., and Rodríguez de la Vega, R. C. (2009) The toxicogenomic multiverse: Convergent recruitment of proteins into animal venoms. *Annu. Rev. Genomics Hum. Genet. 10*, 483−511.